

ELECTROCHEMISTRY

Understanding the electric and nonelectric field components of the cation effect on the electrochemical CO reduction reaction

A. S. Malkani¹, J. Li², N. J. Oliveira¹, M. He², X. Chang¹, B. Xu^{1*}, Q. Lu^{2*}

Electrolyte cations affect the activity of surface-mediated electrocatalytic reactions; however, understanding the modes of interaction between cations and reaction intermediates remains lacking. We show that larger alkali metal cations (excluding the thickness of the hydration shell) promote the electrochemical CO reduction reaction on polycrystalline Cu surfaces in alkaline electrolytes. Combined reactivity and in situ surface-enhanced spectroscopic investigations show that changes to the interfacial electric field strength cannot solely explain the reactivity trend with cation size, suggesting the presence of a nonelectric field strength component in the cation effect. Spectroscopic investigations with cation chelating agents and organic molecules show that the electric and nonelectric field components of the cation effect could be affected by both cation identity and composition of the electrochemical interface. The interdependent nature of interfacial species indicates that the cation effect should be considered an integral part of the broader effect of composition and structure of the electrochemical interface on electrode-mediated reactions.

INTRODUCTION

Electrochemical reduction of CO₂ and CO, a key reaction intermediate in the conversion of CO₂, driven by renewable energy offers an appealing pathway to mitigate the impact of anthropogenic climate change and produce valuable fuels and chemicals (1, 2). The electrochemical CO₂ and CO reduction reactions (CO₂RR and CORR, respectively) are typically conducted in an aqueous electrolyte that supplies the required protons for the reduction. It is well established that Cu is the only monometallic electrocatalyst that can convert CO₂ and CO to C₂₊ hydrocarbons and oxygenates with appreciable activity and selectivity (3). However, substantial improvements in the selectivity for high-value hydrocarbons and oxygenates at lower energy costs, i.e., lower overpotentials, are needed to enhance the economic viability of the CO₂RR and CORR for large-scale implementation. The CO₂RR and CORR occur at the interface between the metallic electrode and the aqueous electrolyte, and thus, the catalytic performance could be influenced by both the electrode surface and electrolyte. Much research effort has been dedicated to the development of electrocatalysts with elaborate compositions and structures to optimize the production of valuable products (4–6). The importance of cations that are electrostatically attracted to the electrochemical interface at reducing potentials in the CO₂RR and CORR has been increasingly recognized recently (7–11), although it was first reported decades ago (12, 13).

Multiple potential pathways through which cations could affect surface-mediated electrocatalytic reactions have been put forward, without a consensus due to the lack of direct experimental evidence. Specific alkali metal cation adsorption has been proposed as a pathway for cations to exert an influence on the hydrogen oxidation reaction on Pt-based catalysts primarily using density functional

theory calculations (14, 15). However, direct experimental evidence for the specific adsorption of cations is lacking, especially below the potential of zero charge (PZC) (16–19). Bell and coworkers (7) proposed that alkali metal cations affected the CO₂RR by modifying the interfacial electric field and stabilizing adsorbed intermediates with substantial dipole moments. Chan and coworkers (8) showed that multiscale modeling was able to achieve impressive agreement with experimental results, supporting the theory that cations affect electrocatalytic reactions by altering the interfacial electric field. According to the Gouy-Chapman-Stern (GCS) double-layer model, the strength of the electric field within the double layer at a given potential below the PZC could be affected by the size of the hydrated cations in the electrolyte, as the center of larger cations cannot get as close to the electrode surface as smaller ones, thus leading to weaker interfacial electric fields. This phenomenon has been previously demonstrated by Roth and Weaver (20) and, more recently, by Waegele and coworkers (21). Their studies used tetraalkylammonium cations of different sizes and determined the Stark tuning rates of the linearly bonded CO on Pt and Cu surfaces, respectively, in the presence of these cations (20, 21). In both cases, the Stark tuning rate, which is representative of the electric field strength, decreases with the increase in cation alkyl chain length (20, 21). However, Waegele and coworkers (21) concluded that the change in the interfacial electric field strength is too small to be the main cause for the observed difference in the CORR activity, which they attributed to the varying interaction between adsorbed CO and interfacial water in the presence of different cations instead. Our recent work on the concentration effect of Na⁺ on the CORR showed that at the same pH, increasing the cation concentration by an order of magnitude (0.1 to 1 M) significantly enhances the reaction rate without changing the Stark tuning rate or the interfacial electric field strength, appreciably (22). This substantial increase in the CORR rates with Na⁺ concentration suggests that the interfacial electric field strength is not the decisive parameter in the conditions investigated (22). Literature discussions have touched upon both the electric and nonelectric field (NEF) strength components of the

Copyright © 2020
The Authors, some
rights reserved;
exclusive licensee
American Association
for the Advancement
of Science. No claim to
original U.S. Government
Works. Distributed
under a Creative
Commons Attribution
NonCommercial
License 4.0 (CC BY-NC).

¹Center for Catalytic Science and Technology, Department of Chemical and Biomolecular Engineering, University of Delaware, Newark, DE 19716, USA. ²State Key Laboratory of Chemical Engineering, Department of Chemical Engineering, Tsinghua University, Beijing 100084, China.

*Corresponding author. Email: bxu@udel.edu (B.X.); luqicheme@mails.tsinghua.edu.cn (Q.L.)

cation effect, albeit in different contexts, i.e., inorganic and organic cations (11, 21). Thus, systematic studies of the cation effect on the CORR encompassing both the electric and NEF strength components are key to understanding their connections and contributions to the cation effect on electrode-mediated reactions in general.

In this work, we show that the nature of alkali metal cations has a significant impact on the rate and the Faradaic efficiency (FE) of the CORR on polycrystalline Cu in alkaline electrolytes. In situ attenuated total reflection surface-enhanced infrared absorption spectroscopy (ATR-SEIRAS; fig. S1) on polycrystalline Cu films shows that cations affect the distribution of sites, i.e., step versus terrace, on which CO adsorbs. Stark tuning rate measurements in the presence of five alkali metal cations show that the electrochemically relevant cation size follows the sequence of $\text{Cs}^+ \cdot x\text{H}_2\text{O} \sim \text{Rb}^+ \cdot x\text{H}_2\text{O} \sim \text{K}^+ \cdot x\text{H}_2\text{O} < \text{Na}^+ \cdot x\text{H}_2\text{O} < \text{Li}^+ \cdot x\text{H}_2\text{O}$, which is in complete agreement with that obtained from correlations verified by transport measurements (23), but is in contrast to that obtained using diffraction methods (24–26). Combined reactivity and spectroscopic investigations show that the interfacial electric field strength estimated by the Stark tuning rate correlates well with the reactivity trend in Li^+ , Na^+ , and K^+ . The Stark tuning rate levels off, but the CORR rate increases as the size of the alkali metal cation increases further from K^+ to Cs^+ , suggesting a NEF strength component in the cation effect. We note that, in this work, the term “cation size” refers to the size of cations without the associated hydration shell, while the size of hydrated cations is denoted as the “electrochemically relevant cation size.” Further spectroscopic investigations with crown ethers and a linear organic ether suggest that the electric and NEF components of the cation effect could be affected by changes to the chemical structure and charge distribution of cations, i.e., the composition of the electrochemical interface. The interdependent nature of interfacial species indicates that the cation effect should be considered as an integral part of the broader effect of composition

and structure of the electrochemical interface on electrode-mediated reactions.

RESULTS

To understand the differences in the CORR activity and selectivity for different alkali metal cation hydroxides, the potential-dependent CO adsorption bands on Cu in alkali metal hydroxides are investigated with SEIRAS. Chemically deposited polycrystalline Cu films on Si ATR crystals, whose composition and morphology have been thoroughly characterized by us and others (27–30), are used as the catalyst. Surface oxygen-containing species, including Cu-O_x and $\text{CuO}_x/(\text{OH})_y$, have been detected at potentials as low as -0.8 V [all voltages in this work are referenced to the reversible hydrogen electrode (RHE) unless noted otherwise] on both the chemically deposited Cu films and commercially available Cu micrometer-sized particles (microparticles) (30). However, they do not appear closely correlated with the CORR activity. The adsorbed CO bands observed in this work correspond well with those reported on metallic Cu surfaces under the ultrahigh vacuum conditions (31–33), and thus, the possibility of CO adsorbed on these oxygen-containing species is not considered. Furthermore, the product distribution in the CORR on the chemically deposited Cu films and Cu microparticles is similar at -0.6 V (30). Thus, the spectral features observed in the SEIRAS experiments should be representative of the surface of Cu microparticles, which are frequently used in the CO_2RR and CORR in both batch and flow configurations (29, 34, 35). Linearly bonded CO (CO_L) SEIRA bands emerge in the >2000 cm^{-1} region (27, 36, 37) and migrate to higher wave numbers as the potential is lowered from -0.1 to -0.5 V in 0.1 M KOH (Fig. 1A, full spectra in fig. S2). This blueshift is contrary to the expected Stark tuning effect, which typically leads to a redshift of CO bands with decreasing potential due to the more effective $d\pi-2\pi^*$ back donation (38–40).

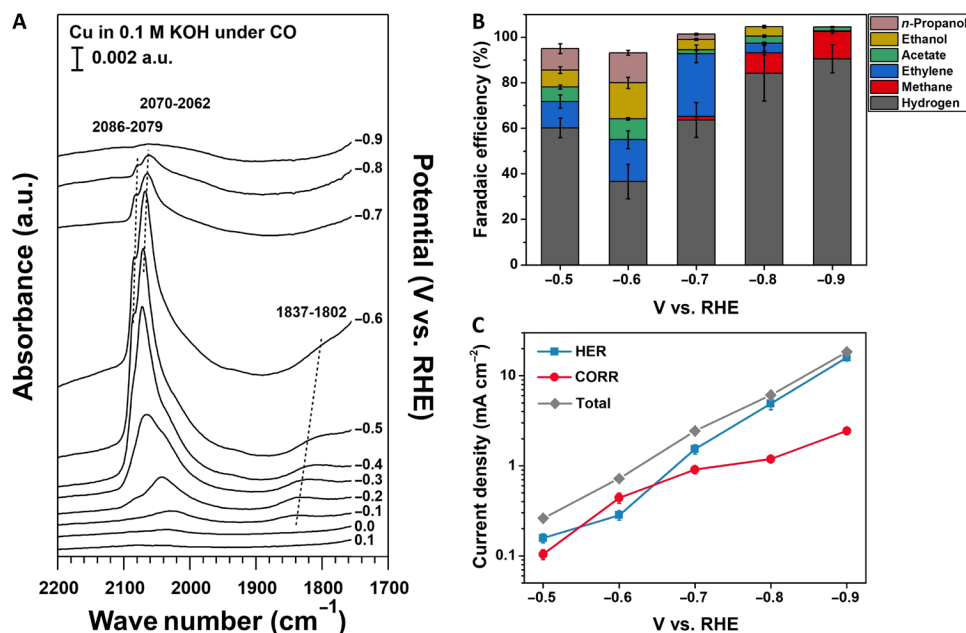


Fig. 1. ATR-SEIRAS spectra and reactivity data in CO-saturated 0.1 M KOH. (A) The traces show the evolution of CO adsorption bands with potential. Spectra presented correspond to 64 coadded scans collected with a 4 cm^{-1} resolution. a.u., arbitrary units. (B) FE and (C) current density of products formed at CORR conditions on polycrystalline Cu foil electrodes. The error bars represent the SD from at least three independent measurements.

Similar blueshifts of CO bands on Cu have been reported at lower pH values and attributed to potential-induced reconstruction of the polycrystalline Cu surface (28). Another possible cause for the blueshift is the increased CO coverage at lower potentials, which leads to dipole-coupling that favors the intensity of the higher wave number bands (32, 41). At more negative potentials, the CO_L band begins to redshift, which could be attributable to the Stark tuning effect. The maximum intensity of the CO_L band is reached at -0.5 V, indicating a saturation CO coverage on the Cu surface. CORR activity at this potential is modest (Fig. 1, B and C) (42), and thus is not expected to affect the CO coverage in any substantial way. The diminished intensity of the CO_L band at potentials below -0.5 V is likely due to the rapid CO consumption in the CORR (Fig. 1, B and C), although the SEIRA spectra are collected in a stirred spectroelectrochemical cell (29). This claim is supported by our recent observation that the intensity of the CO_L band dropped precipitously with a simultaneous enhancement of the competing hydrogen evolution reaction (HER) when stirring is stopped (43). At -0.9 V, the CORR becomes completely mass transport limited due to the high reaction rate and is manifested by the lack of the CO_L band. A shoulder to the CO_L band starts to develop at -0.4 V and becomes increasingly prominent at lower potentials. The lower and higher wave number bands at 2070 and 2087 cm^{-1} at -0.4 V have been assigned to terrace and step sites on Cu surfaces, respectively (31–33). It should be noted that, aside from the major spectroscopic band of linearly bonded CO, a bridge bonded CO band in the 1800 to 1850 cm^{-1} region is also observed (Fig. 1A). However, it has been deemed inactive for the CORR (44) and thus is not discussed further in this work.

The reduced CO coverage on Cu below -0.5 V determined spectroscopically correlates well with the CORR activity on Cu foils in the same potential range. The FE for H_2 increases with the decrease in potential from -0.7 to -0.9 V from 63.6 to 90.6% (Fig. 1B). This is consistent with the diminished CO coverage on Cu at more negative potentials (Fig. 1A) because a larger fraction of the surface is available for the competing HER. The FE for the CORR products is lower at -0.5 V compared to -0.6 V and thus does not follow the trend of decreasing FE with more negative potential. This is likely due to the insufficient overpotential to drive the CORR (42). No spectroscopic feature corresponding to adsorbed H (H_{ad}) is identified, suggesting that H_{ad} has either a very short surface residence time or a low steady-state coverage, or both (45). Among the CORR products, methane becomes increasingly preferred over C_{2+} products as the potential decreases. The FE for methane increases from 1.6% at -0.7 V to 11.9% at -0.9 V, while that of C_{2+} products drops from 36.2 to 2.0% in the same potential range. This correlation could be interpreted in two related ways: (i) a lower CO coverage reduces the probability of the coupling between adsorbed CO on the surface, leading to reduced selectivity for C_{2+} products. Meanwhile, the higher coverage of H_{ad} due to the availability of surface sites facilitates the hydrogenation of adsorbed CO, which enhances the methane production. (ii) Lower electrode potentials intrinsically favor the direct hydrogenation of adsorbed CO, rather than its dimerization (9, 42). Our recent work suggests that the relative selectivity for C_{2+} products is largely insensitive to the overall CO surface coverage on Cu because CO adsorbs in patches (43). Thus, the effect of lower potential is more likely to be the primary driving force for the increased methane selectivity.

Although general potential-dependent features of the CO_L band on Cu in alkali metal hydroxide electrolytes, i.e., LiOH, NaOH,

KOH, RbOH, and CsOH, are similar (Fig. 1A and fig. S3), subtle differences in spectroscopic features reveal the impact of cations on the adsorbed CO. The saturation CO coverage inferred from this band on Cu is reached at -0.5 V for all the equimolar (0.1 M) hydroxide electrolytes having the same pH but different cations. Plotting the spectra with the CO_L band at -0.5 and -0.7 V for each cation (the intensity of CO_L bands at -0.5 V is normalized to account for variations of absolute intensities among independent experiments; Fig. 2A) shows that the decrease in the CO_L band area from -0.5 to -0.7 V increases from $\sim 6\%$ for LiOH to over 40% for the larger alkali metal cation hydroxides (Fig. 2A and fig. S4) (43). Because we have established above that the reduction of the CO_L band at -0.7 V and below is largely caused by the consumption of adsorbed CO via the CORR (43), SEIRAS results suggest that the CORR activity increases with the cation size. This is also consistent with the observation of the CO_L band in LiOH at -0.9 V, which is less prominent in NaOH and absent in KOH, RbOH, and CsOH (Fig. 1A and fig. S3). While the spectra in Fig. 2A show a decrease in peak area of CO on both the step and terrace sites from -0.5 to -0.7 V, our previous work reporting time-resolved spectra under mass transport limitation conditions shows that the step sites are consumed preferentially (43). This agrees with previous literature highlighting that although both CO on terrace and step sites could mediate the CORR, the step sites are orders of magnitude more active (42, 46).

The CORR activity in alkali metal hydroxide electrolytes correlates well with the spectroscopic observation of relative CO coverages at -0.7 V compared to its maximum at -0.5 V. Quantitative assessments of the CORR activity in different alkali metal cation hydroxides on polycrystalline Cu foils are challenging. It has been reported that Cu foils are susceptible to impurities due to their low roughness factors compared to nanostructured alternatives (47). The foils also show low reaction rates under CORR conditions, which necessitates extended reaction times (>30 min) to accumulate product for quantification during which the catalyst is often poisoned (47). As a result, it is unreliable to use activity data on Cu foils in cations with low current densities, e.g., Li^+ and Na^+ , as significantly longer run times (2 to 3 hours) are needed to accumulate sufficient products for accurate quantification (48). This challenge can be partially addressed by preelectrolyzing the already high-purity electrolyte to deposit any remaining metal impurities on a sacrificial cathode before use (detailed in Materials and Methods). Further improvements can be achieved by using recently reported carbon paper supported Cu nanoparticles, which show significantly enhanced stability and reaction rate for the CORR compared to Cu foils (34). At -0.7 V, the current density for C_{2+} products increases almost linearly when the cation in the electrolyte changes from Li^+ to Na^+ and then K^+ , while the increase becomes more gradual from K^+ to Rb^+ and Cs^+ (Fig. 2B). Methane is a minor product for all cations at -0.7 V, while the hydrogen production rate increases gradually from Li^+ to K^+ and accelerates for Rb^+ and Cs^+ (Fig. 2B and fig. S5). Overall, both the CORR and HER accelerate as the size of the cation in the electrolyte increases. This is qualitatively consistent with the spectroscopic observations that the relative CO coverage at -0.7 V relative to its maximum at -0.5 V is inversely correlated to the size of the cation (fig. S4). We note that the CORR reactivity trend in the presence of different alkali metal cations is in general agreement with that for the CO_2RR in bicarbonate electrolytes reported by the Bell group (7). The HER activity increases with cation size (Fig. 2B), while Bell and coworkers reported

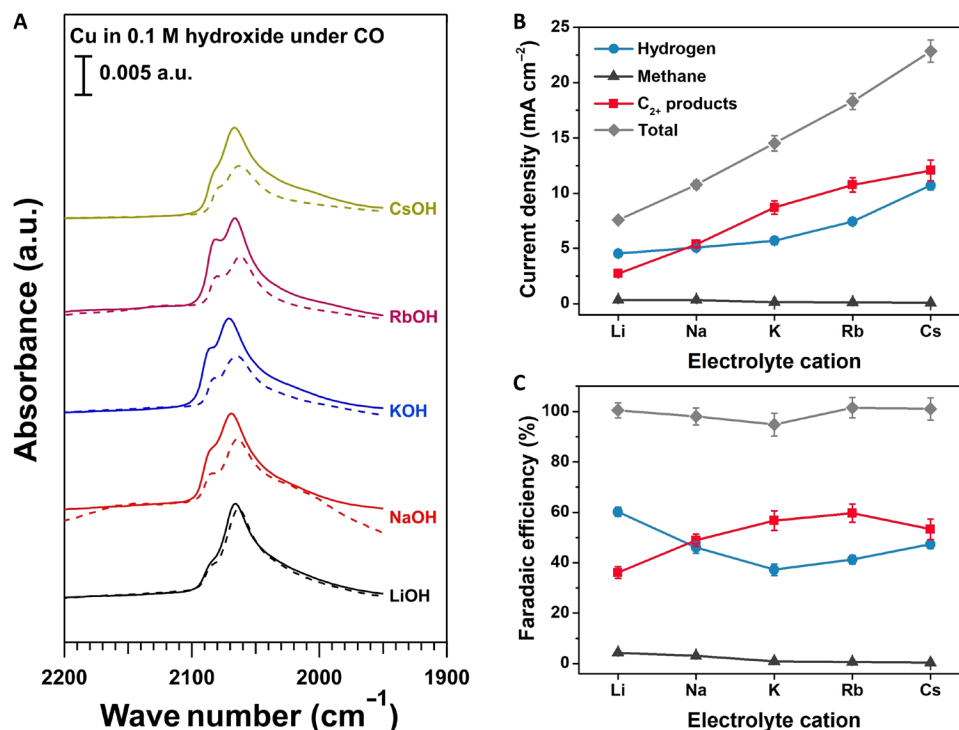


Fig. 2. ATR-SEIRAS spectra and reactivity data in CO-saturated 0.1 M alkali metal hydroxide. (A) The traces show the decrease in linearly bonded CO band intensity from saturation coverage at -0.5 V (solid line) to -0.7 V (dashed line). Spectra presented correspond to 64 coadded scans collected with a 4 cm^{-1} resolution. (B) Current density and (C) FE of products formed at CORR conditions on carbon paper supported Cu microparticles at -0.7 V. The error bars represent the SD from at least three independent measurements. Detailed selectivity plots are provided in fig. S5.

that it is independent of the alkali metal cation size (7). This discrepancy could be attributed to the presence of a different counterion (hydroxide versus bicarbonate) in the electrolyte. Hydroxide-derived oxygen-containing species are known to be present on the copper surface at the CORR conditions (30, 49). Adsorbed hydroxide, along with cations at the outer Helmholtz (OHP), has previously been proposed to affect the water dissociation process needed to release protons for the HER (50).

The distribution of CO adsorbed on terrace and step sites and the Stark tuning rate varies with the size of alkali metal cations. By normalizing the intensity of the CO_L bands at -0.7 V for all cations (Fig. 3), it is clear that the nature of the cation has a significant impact on the distribution of CO adsorbed on terrace and step sites. The shoulder corresponding to CO adsorbed on the step sites of the Cu surface becomes more prominent as the size of the cation increases from Li^+ to K^+ and remains largely unchanged for larger cations, i.e., K^+ , Rb^+ , and Cs^+ . This observation is a direct indication that cations at potentials relevant to the CORR (≤ -0.7 V) actively interact with the surface adsorbed CO and affect their adsorption sites. It is also consistent with our earlier work showing that alkali metal and organic cations can change the distribution of adsorbed CO on atop and bridge sites on Pt (38), as well as Waegle and coworkers' (11) findings reporting the dependence of CO_L band position on the identity of the alkali metal cation. We note that a more quantitative analysis of the spectra regarding the terrace and step site distribution with different cations is complicated by the well-known dynamic dipole coupling effect (33, 51) and thus is not attempted in this work.

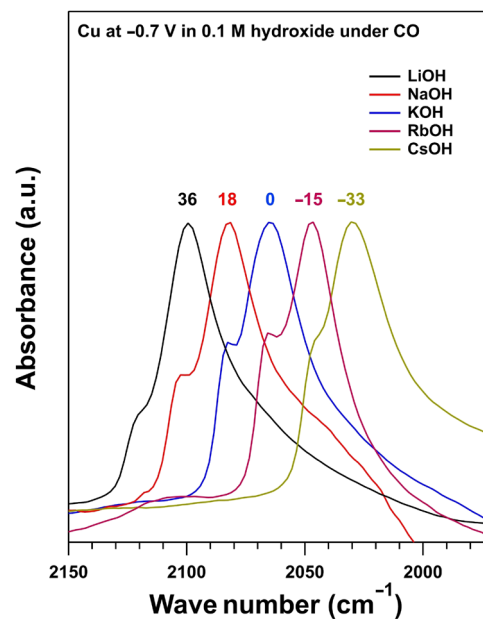


Fig. 3. ATR-SEIRAS spectra in CO-saturated 0.1 M alkali metal cation hydroxide at -0.7 V. The traces show the relative intensity of the linearly bonded CO on the step site band with respect to the normalized peak intensity of the terrace site band. The spectra have been horizontally translated by the wave number mentioned above each trace for clarity. Spectra presented correspond to 64 coadded scans collected with a 4 cm^{-1} resolution.

The measured Stark tuning rates show a distinct trend with the size of hydrated alkali metal cations from that of the bulkier organic cations. The Stark tuning rate increases from 29 to 39 cm^{-1}/V from Li^+ to K^+ and then levels off for larger cations at 39 to 41 cm^{-1}/V (Table 1 and fig. S6), which appears correlated with the site distribution probed by CO adsorption with different alkali metal cations (Fig. 3). It is worth noting that the Stark tuning rate measurements are performed on the anodic sequence of potential steps between -0.7 and -0.3 V, within which the coverage of CO for all cations remains largely unchanged. This is important because the surface reconstruction and changing CO coverage in the cathodic potential steps could contribute to peak shifts (52) and thus complicate the data interpretation. Although a 4 cm^{-1} spectral resolution is used in determining peak positions in SEIRAS, control experiments show that the peak positions obtained with spectral resolutions of 2 and 4 cm^{-1} vary below 1 cm^{-1} (fig. S7). Spectra obtained at a 2 cm^{-1} resolution show poorer signal to noise ratio, and thus, the 4 cm^{-1} spectral resolution is used in all experiments, which is consistent with recent studies (21, 27, 49, 53). According to the GCS double-layer model, the Stark tuning rate reflects the strength of the electric field in the double layer, the change of which causes the shift in vibrational bands (54). Waegele and coworkers (21) recently showed that the Stark tuning rate decreased with the increasing size of tetraalkylammonium cations, which was rationalized by the correlation of increased thickness of the double layer with the size of cations with the GCS model. The situation is more complex for alkali metal cations, as the electrochemically relevant size of these cations in aqueous electrolytes is defined and determined in multiple ways, resulting in opposite trends. Crystal ionic radii of alkaline cations are determined on the basis of lattice constants of various crystals containing these cations, which do not take the hydration shell of the cation into account (24, 55), and thus are unlikely to reflect the effective size of cations at the electrochemical interface. The position of the first maximum in the radial distribution function of the ion-water distance could be a more reliable representative measure of the effective size of ions (24–26). The size of hydrated cations has been determined by diffraction methods (24–26), which typically agrees with older computational investigations (56, 57). The sizes of

hydrated Li^+ , Na^+ , K^+ , and Cs^+ are determined to be 2.1, 2.4, 2.7, and 3.13 Å, respectively (24), which are expected to lead to a decreasing trend of Stark tuning rates. However, measured Stark tuning rates for these cations show the opposite trend (Table 1). This inconsistency could be attributed to the fact that these sizes of hydrated cations only reflect the distance between the ion and the first layer of the hydration shell. However, smaller cations like Li^+ have a more concentrated charge and consequently a thicker hydration shell than larger cations such as Cs^+ . The hydration shell around the relatively hydrophobic alkyl ammonium cations is relatively weakly bound to the cation, and thus, the size of these organic cations relevant in electrochemistry is similar to that without including the hydration shell (58). Extended hydration shells are difficult to detect with diffraction methods due to the weak interaction with the cation; however, they could still affect interfacial electrochemistry and thus should be considered electrochemically relevant. Within the GCS framework, the measured Stark tuning rates could be used to determine the relative electrochemically relevant sizes of hydrated alkali metal cations, i.e., a higher Stark tuning rate corresponds to a thinner double layer and smaller hydrated cations. The following size ranking of hydrated alkali metal cations can be obtained by the measured Stark tuning rates: $\text{Cs}^+ \cdot x\text{H}_2\text{O} \sim \text{Rb}^+ \cdot x\text{H}_2\text{O} > \text{K}^+ \cdot x\text{H}_2\text{O} > \text{Na}^+ \cdot x\text{H}_2\text{O} > \text{Li}^+ \cdot x\text{H}_2\text{O}$. This sequence is in complete agreement with Robinson and Stokes' empirical correlations, which were validated by transport properties such as the temperature coefficient of equivalent conductance, the viscosity β -coefficient, and the partial molar ionic entropy (23), and is also similar to a recent computational trend predicted and validated by Stark shift values at a fixed potential on Pt (8). This trend is also consistent with literature that suggests that monovalent cations with more concentrated charges tend to have a longer range impact on surrounding water molecules (59). This size sequence shows that the electrochemically relevant hydrated cations, especially for Li^+ and Na^+ , are likely to have hydration shells with more than one layer of water molecules. The similarity between the trend in the Stark tuning rate (Table 1) and the distribution of CO_L bands on terrace and step sites (Fig. 3) suggests a shared origin. One possible explanation is that as the size of the hydrated cations decreases from Li^+ to K^+ , the repulsive interaction between the hydrated cations and the adsorbed CO increases, which pushes adsorbed CO from terrace to step sites due to the better accessibility of terrace sites for hydrated cations (38). This interpretation entails that both the stronger interfacial electric field and the redistribution of CO adsorption sites are consequences of the cation structure, rather than the interfacial electric field alone driving changes in CO adsorption sites. The remaining CO on terrace sites could be stabilized by the cations as previously suggested by Bell and coworkers (7), which leads to the redshifted peak position with increasing cation size (Table 1). Following the same reasoning, the site distribution and peak position for adsorbed CO with K^+ , Rb^+ , and Cs^+ are similar because the average distance between these cations and the electrode surface does not vary substantially.

The reactivity and spectroscopic trends with Li^+ , Na^+ , and K^+ suggest that increased electric field strength with decreasing size of the hydrated cations is likely responsible for the enhanced C-C coupling activity (Fig. 2). Bell and coworkers (7) rationalized this activity trend by arguing that the larger cations (without including the hydration shell) have higher concentrations at the OHP that stabilize CO and C-C coupling intermediates. Results presented above are consistent with this hypothesis as larger cations stabilize the CO on

Table 1. Cation-dependent spectroscopic trends. Stark tuning rate and peak position of the linearly bonded CO on terrace site band in CO-saturated 0.1 M hydroxide.

Cation in 0.1 M hydroxide	Stark tuning rate (cm^{-1}/V) ^a	Peak position at -0.7 V (cm^{-1}) ^a
Li^+	29	2068
Na^+	32	2066
K^+	39	2063
Rb^+	41	2062
Cs^+	40	2062
C- K^+	28	2060
T- Na^+	28	2064
C- Na^+	25	2060

^aStark tuning rate and peak positions vary within ± 1 unit for the three independent replicates performed with each cation.

terrace sites and direct adsorbed CO from terrace to step sites, which have been shown to be more favorable for the C-C coupling pathway (42, 46). This is also supported by the measured Stark tuning rates that vary in sync from Li^+ to K^+ .

Comparison between the spectroscopic and reactivity results for larger alkali metal cations, i.e., K^+ , Rb^+ , and Cs^+ , suggests a mode of interaction between cations and reaction intermediates independent of the electrostatic effects determined by the Stark tuning rate. The hypothesis regarding the size of hydrated cations, and in turn interfacial electric field strength, discussed above cannot explain the reactivity trend observed for K^+ , Rb^+ , and Cs^+ (Fig. 2B), as the overall current density increases with the cation size while the spectroscopic features (including the Stark tuning rate) remain largely unchanged (Fig. 3 and Table 1). This indicates that the electric field strength is not the only mechanism through which cations affect the surface-mediated reaction.

The impact of nonelectrostatic interactions, as well as the correlation of the size of hydrated cations with CO adsorption sites and Stark tuning rates, is further supported by changing the nature of

cations through chelation. 18-Crown-6 is a crown ether known to effectively chelate an equimolar solution of K^+ ions (60). Thus, the nature of the cation can largely be changed by introducing the crown ether to the KOH electrolyte (crown: K^+ = 1:1) to form a chelated complex, referred to as C- K^+ (Fig. 4A). Upon the introduction of equimolar crown ether to 0.1 M KOH at -0.4 V, the CO_L band corresponding to the step sites disappears while the intensity of the CO_T band corresponding to the terrace sites increases slightly (Fig. 4B). The CO_T band position is also redshifted by 2 cm^{-1} upon introducing the crown ether (based on two identical repeats). Control experiments in 0.1 M tetramethylammonium (TMAOH), an organic cation too bulky to be chelated by the crown ether, show that the introduction of the crown ether has a less prominent impact on the CO_T band on step sites and causes no detectable shift in peak position of CO adsorbed on the terrace sites (fig. S8). This observation supports the hypothesis that the nature of cations in the electrolyte directly affects the surface sites available for CO adsorption. We do not observe a Stark tuning effect on the crown ether bands, which is consistent with our previous studies (19, 22) and

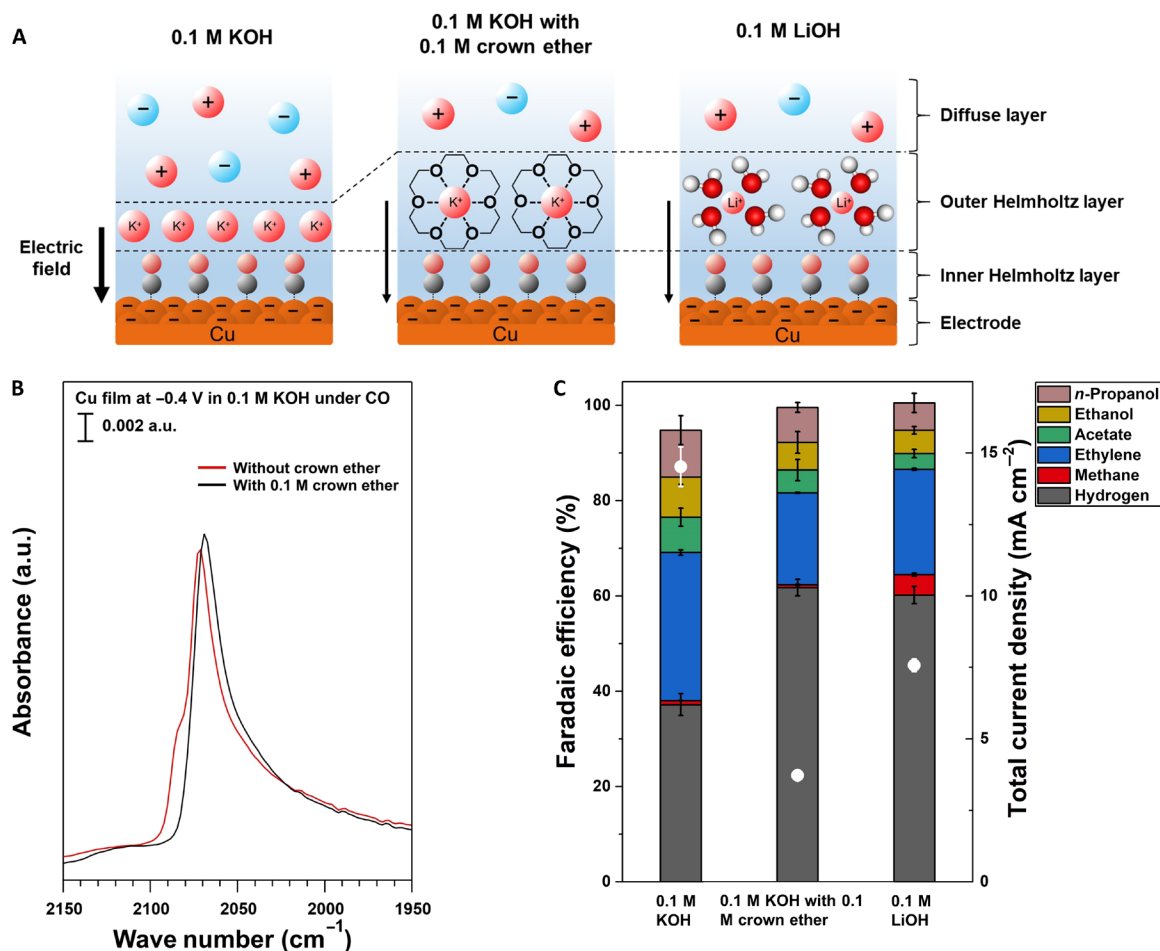


Fig. 4. The impact of chelating K^+ cations. (A) Increasing the electrochemically relevant cation size, either by chelation (middle, C- K^+) or by using a cation with a large hydration shell (right, Li^+), expands the outer Helmholtz layer. This reduces the cation-dependent electric field intensity whose strength is represented by the thickness of the black arrow to the left of each panel. (B) ATR-SEIRAS spectra in CO-saturated 0.1 M KOH at -0.4 V before and after adding equimolar crown ether showing the crown ether's impact on linearly bonded CO binding sites and peak intensity. Spectra presented correspond to 64 coadded scans collected with a 4 cm^{-1} resolution. (C) Reactivity data at -0.7 V, in 0.1 M KOH with and without crown ether, and 0.1 M LiOH showing the impact of crown ether on product distribution and rate. The stacked bars and the white dots indicate FE (left axis) and total current density (right axis), respectively. The error bars represent the SD from at least three independent measurements.

suggests that C-K⁺ does not specifically adsorb to Cu sites but affects the surface-bound CO from the electrolyte (fig. S9A). Furthermore, the lack of the CO_L band on the step sites with C-K⁺ is reminiscent of the spectrum in LiOH, indicating that C-K⁺ favors terrace sites for adsorbed CO, similar to Li⁺. This is expected as C-K⁺, which resembles hydrated Li⁺ (Fig. 4A), is bulkier than K⁺, given that the size of the cavity in 18-crown-6 matches that of the K⁺ cation (61). It follows that C-K⁺ does not interact with adsorbed CO_L sufficiently strongly to affect their adsorption configuration, e.g., pushing a fraction of them to step sites. The Stark tuning rate of the CO_L band reduces from 39 to 28 cm⁻¹/V after the introduction of the crown ether to the KOH solution (fig. S9B), which is similar to the difference in the Stark tuning rates between KOH and LiOH (Table 1). The similar Stark tuning rates of C-K⁺ (28 cm⁻¹/V) and hydrated Li⁺ (29 cm⁻¹/V) indicate that they have similar electrochemically relevant cation sizes.

We hypothesize that there is a NEF component in the cation effect on the CORR, which is largely dependent on the nature and structure of the cation. Reactivity results with Li⁺ and C-K⁺ (Fig. 4C) show that the FE toward the CORR and the HER are ~40 and ~60%, respectively, for both cations, but the total current density in LiOH is a factor of 2 greater than that of C-K⁺ (~7.6 mA/cm² versus ~3.7 mA/cm²; Fig. 4C). This result suggests that the electric field intensity correlates better with the FE toward the CORR rather than the rate. The plateauing of the CORR FE curve (Fig. 2C) and Stark tuning rates (Table 1) for K⁺, Rb⁺, and Cs⁺, as well as the monotonic increase in the total current density from K⁺ to Cs⁺, supports this interpretation (Fig. 2B). Our recent work on the cation concentration effect at the same pH on the CORR activity also showed that the formation rate, rather than the FE, of the CORR products grows with the increasing cation (Na⁺) concentration, while the Stark tuning rate remains independent of the cation concentration (22). Combined, these results point to a NEF component in the cation effect on the electrocatalytic reactions that primarily affects the reaction rate. The NEF component for alkali metal cations appears more directly related to the nature/structure of hydrated cations than their interaction with the surface adsorbed species. Peak positions of terrace-site adsorbed CO with K⁺, Rb⁺, and Cs⁺ are identical within experimental errors (± 1 cm⁻¹; Table 1), and the overall line-shapes of the CO bands for these cations are also similar (Fig. 3), suggesting comparable interactions of these cations with the adsorbed CO. The primary difference among these cations is likely the increasingly looser association with the hydration shell as the size of the naked alkali metal cation increases. In addition, the comparison between Li⁺ and C-K⁺ highlights the impact of the structure of cations. On the basis of the similar Stark tuning rates, hydrated Li⁺ and C-K⁺ are expected to have similar interfacial electric field strength and electrochemically relevant sizes, albeit with different structures. The size of hydrated Li⁺ is largely defined by the extended hydration shell, while the diffuse charge of C-K⁺ and the relatively hydrophobic ether likely lead to a loosely bound and thin hydration shell. Thus, the differences in the CO peak position (2068 cm⁻¹ for Li⁺ versus 2060 cm⁻¹ for C-K⁺ at -0.7 V) and the overall lineshapes of the adsorbed CO bands are likely attributable to the markedly different structure of the cations. This, in turn, leads to different interactions with adsorbed CO. A common theme appears to be the immediate environment around alkali metal cations, i.e., chelating agent, hydration shells, and, more generally, the interfacial water. This is consistent with the cation concentration effect reported in

our recent work in that higher Na⁺ concentrations will certainly change the interfacial water structure (22), as an increasing fraction of the interfacial water molecules is tied up to the hydration shell of cations.

The employment of a nonchelating ether in spectroscopic investigations highlights that the electric and NEF effects of cations can also be produced by introducing a neutral species to the electrochemical interface. Tetraethylene glycol dimethyl ether (tetraglyme) is an ether molecule with similar molecular weight and functional groups to 15-Crown-5, a crown ether that selectively chelates Na⁺ cations (61), but without the capability of chelating cations due to its linear structure. 15-Crown-5 and tetraglyme are expected to interact with the interfacial water similarly due to their similar functional groups but differently with cations, i.e., the former chelates Na⁺, changing the nature of the cation, while the latter does not. The CO_L band position in Na⁺, equimolar tetraglyme and Na⁺ (T-Na⁺), and equimolar 15-crown-5 and Na⁺ (C-Na⁺) decreases in the sequence Na⁺ (2066 cm⁻¹) > T-Na⁺ (2064 cm⁻¹) > C-Na⁺ (2060 cm⁻¹), and so does the ratio of CO on step versus terrace sites (Table 1 and Fig. 5). The shift in the CO_L peak position and site distribution with T-Na⁺ relative to Na⁺ could be attributed to either tetraglyme's interaction with adsorbed CO or the disruption of the interaction between CO and other interfacial species, e.g., Na⁺, by the presence of tetraglyme. Specific interaction between adsorbed CO and alkali metal cations has been previously proposed in non-aqueous electrolytes (20). Because tetraglyme is a neutral species and does not chelate Na⁺, its interaction with adsorbed CO is chemical in nature, rather than driven by the electrode potential. The fact that the peak shift with T-Na⁺ versus Na⁺ (2 cm⁻¹) is smaller than

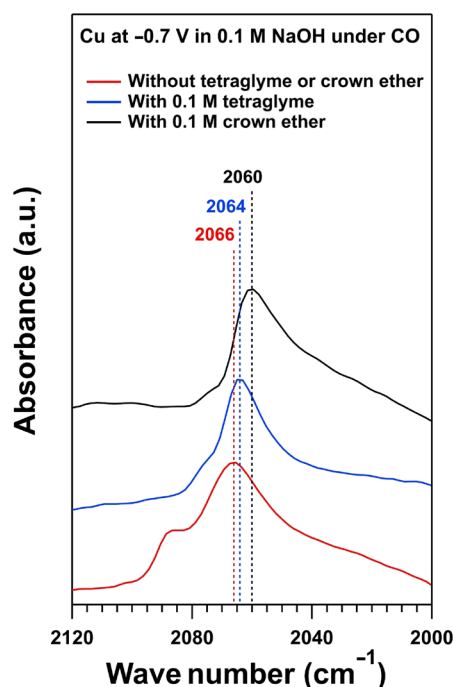


Fig. 5. The impact of organics on ATR-SEIRAS spectra. The traces show the linearly bonded CO on terrace site peak position and the relative intensity of the step site band with respect to the normalized peak intensity of the terrace site band in CO-saturated 0.1 M sodium hydroxide at -0.7 V. Spectra presented correspond to 64 coadded scans collected with a 4 cm⁻¹ resolution.

that of C-Na⁺ versus Na⁺ (6 cm⁻¹) could be attributed to the ability of C-Na⁺ to get closer to the electrode surface than tetraglyme at negative potentials due to the electrostatic attraction. The Stark tuning rate also decreases in the sequence Na⁺ (32 cm⁻¹/V) > T-Na⁺ (28 cm⁻¹/V) > C-Na⁺ (25 cm⁻¹/V) (Table 1 and figs. S6 and S10). The introduction of tetraglyme reduces the Stark tuning rate, i.e., the interfacial electric field strength, without changing the identity of cations, albeit to a lesser extent than C-Na⁺. The impact of tetraglyme on the strength of the interfacial field strength could be rationalized via the analogy of the modification of the dielectric constant of an aqueous solution by the introduction of organic species. However, dielectric constant at the length scale of typical electrochemical interfaces, especially the distance between the OHP and the electrode surface (<<10 nm), is not well defined. Thus, both the electric and the NEF components of the cation effect can be modified by a neutral species (tetraglyme) without any strong interaction with cations. This suggests that the effects induced by cations on the properties of the electrochemical interface and surface-mediated reactions are not unique. The low concentration of unchelated 15-Crown-5 is unlikely to have an appreciable impact on the spectroscopic features of the C-Na⁺ system. This is because even with equimolar tetraglyme (chemically similar to 15-Crown-5) and Na⁺, the T-Na⁺ system shows quite different spectral features compared to the C-Na⁺ one (Fig. 5). There is also no consistent correlation between the CO_L peak position and the Stark tuning rate among the cations investigated (Table 1), suggesting that the peak shift caused by cations is likely via the NEF mode of interaction.

Results presented in this work suggest that the cation effect is best viewed as an inseparable part of interfacial effect, as it could be conceptually convoluted and unnecessary to separate cations from the rest of the electrochemical interface. The key difference among Na⁺, T-Na⁺, and C-Na⁺ is how Na⁺ interacts with species in its immediate environment, i.e., water, chelating or nonchelating organics. C-Na⁺ could be viewed as either a distinct cation from Na⁺ or a guest cation within its surrounding organic host species. Because of the strong host-guest interaction, it is reasonable to consider C-Na⁺ as a different cation from Na⁺. It follows that Na⁺ and its hydration shell together should also be considered as a cation due to their strong interaction, rather than Na⁺ with a few surrounding water molecules. This is consistent with our results that the electrochemically relevant size of alkali metal cations is the size of their hydrated counterparts. Attempts to separate cations from the rest of interfacial species, especially in concentrated electrolytes, could prove impractical as it has been reported that in a 2 M NaCl solution, there is no space for “free water” between the hydrated ions (58). The electrochemical interface in a concentrated electrolyte appears to consist of only hydrated ions, which entails that at negative potentials, the cation effect becomes synonymous with the interfacial effect. A recent computational study suggests that the concentration of K⁺ close to the electrode surface could be as high as 1.5 M at negative potentials in a 0.1 M K⁺ electrolyte (62). This supports the hypothesis that the electrochemical interfacial area is crowded with cations even in relatively dilute bulk electrolytes at negative potentials. It follows that cations should be considered as an integral part of the electrochemical interface, in which all species are highly connected and can affect the properties of the electrochemical interface and surface-mediated reactions via both electric and NEF related modes. The understanding of these modes

through which inorganic and organic cations interact with surface-bound intermediates and affect surface-mediated electrocatalytic reactions could enable targeted engineering of electrochemical interfaces for specific reactions, such as the CO₂RR and CORR.

CONCLUSION

In this work, we show that the nature of the alkali metal cation has a significant impact on the activity and product distribution of the CORR on a polycrystalline Cu surface in alkaline electrolytes. Rates of both the CORR and the competing HER increase monotonically with the size of the cation without accounting for its hydration shell. The FE for CORR products increases from Li⁺ to K⁺ and remains largely constant for the larger cations. Spectroscopic investigations reveal that different cations lead to varied CO adsorption site distributions on Cu, with the fraction of CO adsorbed on step sites, relative to that on terrace sites, increasing from Li⁺ to K⁺ and then leveling off for the larger cations. This trend coincides with the measured Stark tuning rates of adsorbed CO in the presence of these cation-containing electrolytes, suggesting a shared origin. On the basis of the GCS double-layer framework, the measured Stark tuning rates indicate that the electrochemically relevant size of hydrated alkali metal cations, and in turn the thickness of the double layer, follows the following sequence: Cs⁺·xH₂O ~ Rb⁺·xH₂O ~ K⁺·xH₂O < Na⁺·xH₂O < Li⁺·xH₂O. Combined reactivity and SEIRAS investigations demonstrate that there are both electric and NEF components of the cation effect. The interfacial electric field strength is largely responsible for the increasing trend in the CORR reactivity from Li⁺ to K⁺, while the plateauing Stark tuning rate and the rising CORR rate with K⁺, Rb⁺, and Cs⁺ suggest a NEF strength component in the cation effect. Spectroscopic investigations with crown ethers and tetraglyme show that the electric and NEF components of the cation effect could be affected by changes to the chemical structure and charge distribution of cations. The close interplay of various species, including cations, at the electrochemical interface suggests that the cation effect should be considered as an integral part of the general effect of composition and structure of the electrochemical interface on electrode-mediated reactions.

MATERIALS AND METHODS

Spectroscopic studies

Setup

The spectroelectrochemical setup used has been described in the supporting information section of our previous works (29, 43). It resembled a typical electrochemical H-cell with the capability of stirring to mimic reaction conditions while collecting spectroscopic information (fig. S1). One compartment contained a graphite counter electrode (CE; fine extruded graphite rod, Graphite Store) and was separated from the other by a Nafion ion exchange membrane (Nafion 211, Fuel Cell Store). The other compartment contained the working electrode (Cu film), an Ag/AgCl reference electrode (3.0 M NaCl, BASi), and gas inlet and purge lines. The electrodes were connected to a potentiostat (Solartron 1260/1287) that was used for electrochemical measurements. The cell was integrated into the Agilent Technologies Cary 660 FTIR spectrometer equipped with a liquid nitrogen-cooled mercury cadmium telluride (MCT) detector and a polarizer in the p-polarized light setting.

Cu film electrode

The chemically deposited Cu film preparation process was adapted from Gunathunge *et al.* (28) and has been described in detail in our earlier work too (29). The roughness factor of the chemically deposited Cu films varies between 10 and 12 (27, 28). Atomic force microscopy (AFM) results show that the as-prepared Cu film has a faceted island morphology with a thickness of ~80 nm (27). Scanning electron microscopy images before and after potential steps in hydroxide show no difference in particle size (29). X-ray diffraction patterns of the as-deposited Cu film show the presence of the (111) and (200) Cu facets (30), but polycrystalline Cu is known to undergo reconstruction in alkaline conditions at reducing potentials and oxidation when exposed to air, making its thorough characterization challenging (63).

Electrolyte

A 0.1 M alkali metal/organic cation hydroxide solution (Sigma-Aldrich, $\geq 99.9\%$), preelectrolyzed for 24 hours using a constant reducing current of -5 mA cm^{-2} to deposit most of the metal impurities onto a Cu foil (Sigma-Aldrich, 99.998%), was used as the electrolyte for the spectroscopic tests. For the experiments involving the use of crown ether (18-crown-6, Acros Organics, 99.0% or 15-crown-5, Sigma-Aldrich, 98%) or tetraglyme (Sigma-Aldrich, $\geq 99\%$), they were directly added to the hydroxide electrolyte in an equimolar portion.

Reactivity studies

Setup

A Gamry Reference 600+ potentiostat was used for all electrochemical measurements. All electrolysis experiments were conducted in a highly anti-alkali all-poly(methyl methacrylate) (PMMA) two-compartment electrochemical cell separated by piece of anion-conducting membrane (Selemon AMV AGC Inc.) (fig. S11). A graphite rod (Sigma-Aldrich, 99.999%) was used as the CE. Potentials were measured against an Hg/Hg₂Cl₂ reference (saturated KCl, BASi), which was calibrated using a homemade standard hydrogen electrode. The measured potential was converted to the RHE reference scale using the following equation: Potential (vs. RHE) = Potential (vs. Hg/Hg₂Cl₂) + 0.241 V + 0.0591 V \times pH.

CO gas (Air Liquide, 99.999%) was delivered into the electrolyte through a gas dispersion frit to ensure sufficient gas-electrolyte mixing at a flow rate of $10.00 \text{ cm}^3 \text{ min}^{-1}$. The flow rate was controlled by a mass flow controller (MKS Instruments Inc.) and calibrated using an ADM flow meter from Agilent Technologies. The headspace gas was vented directly into the sampling loop of a gas chromatograph (Agilent 7890B) and quantified every 17 min for gas-phase products. Liquid products were quantified by a Bruker AVIII 400-MHz nuclear magnetic resonance (NMR) spectrometer. Typically, the NMR sample was prepared by mixing 500 μl of the electrolyte with 100 μl of D₂O (Sigma-Aldrich, 99.9%) and 1.67 ppm (m/m) dimethyl sulfoxide (Alfa Aesar, $\geq 99.9\%$) as an internal standard. The water signal was suppressed using the presaturation method. The uncompensated resistance (R_u) was determined by potentiostatic electrochemical impedance spectroscopy. The potentiostat compensated for 85% of R_u during the electrolysis, and the remaining 15% was manually corrected for afterward to arrive at the actual potential.

Cu foil electrode

Cu foils (Alfa Aesar, 0.1 mm thick, 99.9999%) were first mechanically polished using sandpaper (P1200, STARCKE) and then elec-

tropolished in 85% ortho-phosphoric acid (Sigma-Aldrich, 85% in water) at 2.1 V versus a graphite rod (Sigma-Aldrich, 99.999%) CE for 5 min. After rinsing with Milli-Q water (18.2 megohm-cm), Cu foils were dried under a vacuum. Then, a Cu wire current collector was attached to one end of the electrode using silver epoxy.

Polycrystalline Cu microparticle electrode

Eight milligrams of Cu microparticles (Sigma-Aldrich, $<45 \mu\text{m}$, 99.7%) was uniformly dispersed onto an 8 cm² Sigracet 39 BC (Fuel Cell Store) carbon paper to achieve a catalyst loading of approximately 1.0 mg cm^{-2} . Next, 200 μl of a 2.5 weight % Nafion solution (Sigma-Aldrich) was uniformly deposited onto the catalyst layer. After drying in air, the catalyst was further dried under vacuum to thoroughly remove the residual solvent. Then, the catalyst was cut into individual electrodes that were approximately $0.5 \times 1.5 \text{ cm}^2$. A nickel wire current collector was subsequently attached to one end of the electrode using silver epoxy. Before CO electroreduction, all electrodes were pretreated at -0.7 V for 5 min in an argon (Air Liquide, 99.999%)–purged electrolyte to stabilize the surface conditions.

Electrolyte

Lithium hydroxide monohydrate (99.995% metals basis) was purchased from Alfa Aesar. Sodium hydroxide (semiconductor grade, 99.99% trace metals basis) was purchased from Sigma-Aldrich. Potassium hydroxide (semiconductor grade, 99.99% trace metals basis) was purchased from Sigma-Aldrich. Rubidium hydroxide hydrate (15 to 20% H₂O, 99% metals basis) was purchased from Alfa Aesar. Cesium hydroxide monohydrate (99.95% trace metals basis) was purchased from Sigma-Aldrich. The electrolytes used for all reactivity studies were purified with Chelex resin (Sigma-Aldrich, Chelex 100 sodium form). To further remove the trace metal contamination in 0.1 M RbOH, preelectrolysis of the electrolyte in an Ar atmosphere was carried out for 2 hours using electropolished Cu foil electrodes at a constant current density of -5 mA cm^{-2} . The electrolyte pH, which was detected using the Orion Star A111 Benchtop pH Meter (Thermo Fisher Scientific), showed no significant change after the electrolysis.

SUPPLEMENTARY MATERIALS

Supplementary material for this article is available at <http://advances.sciencemag.org/cgi/content/full/6/45/eabd2569/DC1>

REFERENCES AND NOTES

1. S. Nitopi, E. Bertheussen, S. B. Scott, X. Liu, A. K. Engstfeld, S. Horch, B. Seger, I. E. L. Stephens, K. Chan, C. Hahn, J. K. Nørskov, T. F. Jaramillo, I. Chorkendorff, Progress and perspectives of electrochemical CO₂ reduction on copper in aqueous electrolyte. *Chem. Rev.* **119**, 7610–7672 (2019).
2. J.-P. Jones, G. K. S. Prakash, G. A. Olah, Electrochemical CO₂ reduction: Recent advances and current trends. *Isr. J. Chem.* **54**, 1451–1466 (2014).
3. Y. Hori, Electrochemical CO₂ reduction on metal electrodes, in *Modern Aspects of Electrochemistry*, C. G. Vayenas, R. E. White, M. E. Gamboa-Aldeco, Eds. (Springer, 2008), vol. 42, pp. 89–189.
4. J. E. Pander III, D. Ren, Y. Huang, N. W. X. Loo, S. H. L. Hong, B. S. Yeo, Understanding the heterogeneous electrocatalytic reduction of carbon dioxide on oxide-derived catalysts. *ChemElectroChem* **5**, 219–237 (2018).
5. H. S. Jeon, S. Kunze, F. Scholten, B. Roldan Cuenya, Prism-shaped Cu nanocatalysts for electrochemical CO₂ reduction to ethylene. *ACS Catal.* **8**, 531–535 (2018).
6. F. S. Roberts, K. P. Kuhl, A. Nilsson, Electroreduction of carbon monoxide over a copper nanocube catalyst: Surface structure and pH dependence on selectivity. *ChemCatChem* **8**, 1119–1124 (2016).
7. J. Resasco, L. D. Chen, E. Clark, C. Tsai, C. Hahn, T. F. Jaramillo, K. Chan, A. T. Bell, Promoter effects of alkali metal cations on the electrochemical reduction of carbon dioxide. *J. Am. Chem. Soc.* **139**, 11277–11287 (2017).
8. S. Ringe, E. L. Clark, J. Resasco, A. Walton, B. Seger, A. T. Bell, K. Chan, Understanding cation effects in electrochemical CO₂ reduction. *Energ. Environ. Sci.* **12**, 3001–3014 (2019).

9. E. Pérez-Gallent, G. Marcandalli, M. C. Figueiredo, F. Calle-Vallejo, M. T. M. Koper, Structure- and potential-dependent cation effects on CO reduction at copper single-crystal electrodes. *J. Am. Chem. Soc.* **139**, 16412–16419 (2017).
10. M. R. Singh, Y. Kwon, Y. Lum, J. W. Ager III, A. T. Bell, Hydrolysis of electrolyte cations enhances the electrochemical reduction of CO₂ over Ag and Cu. *J. Am. Chem. Soc.* **138**, 13006–13012 (2016).
11. C. M. Gunathunge, V. J. Ovalle, M. M. Waegle, Probing promoting effects of alkali cations on the reduction of CO at the aqueous electrolyte/copper interface. *Phys. Chem. Chem. Phys.* **19**, 30166–30172 (2017).
12. A. N. Frumkin, Influence of cation adsorption on the kinetics of electrode processes. *Trans. Faraday Soc.* **55**, 156–167 (1959).
13. W. Paik, T. N. Andersen, H. Eyring, Kinetic studies of the electrolytic reduction of carbon dioxide on the mercury electrode. *Electrochim. Acta* **14**, 1217–1232 (1969).
14. I. T. McCrum, X. Chen, K. A. Schwarz, M. J. Janik, M. T. M. Koper, Effect of step density and orientation on the apparent pH dependence of hydrogen and hydroxide adsorption on stepped platinum surfaces. *J. Phys. Chem. C* **122**, 16756–16764 (2018).
15. X. Chen, I. T. McCrum, K. A. Schwarz, M. J. Janik, M. T. M. Koper, Co-adsorption of cations as the cause of the apparent pH dependence of hydrogen adsorption on a stepped platinum single-crystal electrode. *Angew. Chem. Int. Ed.* **56**, 15025–15029 (2017).
16. D. Strmcnik, D. F. van der Vliet, K.-C. Chang, V. Komanicky, K. Kodama, H. You, V. R. Stamenkovic, N. M. Marković, Effects of Li⁺, K⁺, and Ba²⁺ cations on the ORR at model and high surface area Pt and Au surfaces in alkaline solutions. *J. Phys. Chem. Lett.* **2**, 2733–2736 (2011).
17. M. Nakamura, Y. Nakajima, N. Hoshi, H. Tajiri, O. Sakata, Effect of non-specifically adsorbed ions on the surface oxidation of Pt(111). *ChemPhysChem* **14**, 2426–2431 (2013).
18. M. Nakamura, Y. Nakajima, K. Kato, O. Sakata, N. Hoshi, Surface oxidation of Au(111) electrode in alkaline media studied by using X-ray diffraction and infrared spectroscopy: Effect of alkali metal cation on the alcohol oxidation reactions. *J. Phys. Chem. C* **119**, 23586–23591 (2015).
19. X. Yang, J. Nash, N. Oliveira, Y. Yan, B. Xu, Understanding the pH dependence of underpotential deposited hydrogen on platinum. *Angew. Chem. Int. Ed.* **58**, 17718–17723 (2019).
20. J. D. Roth, M. J. Weaver, Role of double-layer cation on the potential-dependent stretching frequencies and binding geometries of carbon monoxide at platinum-nonaqueous interfaces. *Langmuir* **8**, 1451–1458 (1992).
21. J. Li, X. Li, C. M. Gunathunge, M. M. Waegle, Hydrogen bonding steers the product selectivity of electrocatalytic CO reduction. *Proc. Natl. Acad. Sci. U.S.A.* **116**, 9220–9229 (2019).
22. J. Li, D. Wu, A. S. Malkani, X. Chang, M.-J. Cheng, B. Xu, Q. Lu, Hydroxide is not a promoter of C₂-product formation in the electrochemical reduction of CO on copper. *Angew. Chem. Int. Ed.* **59**, 4464–4469 (2020).
23. E. R. Nightingale Jr., Phenomenological theory of ion solvation. Effective radii of hydrated ions. *J. Phys. Chem.* **63**, 1381–1387 (1959).
24. Y. Marcus, Ionic radii in aqueous solutions. *Chem. Rev.* **88**, 1475–1498 (1988).
25. H. Ohtaki, T. Radnai, Structure and dynamics of hydrated ions. *Chem. Rev.* **93**, 1157–1204 (1993).
26. J. Mähler, I. Persson, A study of the hydration of the alkali metal ions in aqueous solution. *Inorg. Chem.* **51**, 425–438 (2012).
27. A. Wuttig, C. Liu, Q. Peng, M. Yaguchi, C. H. Hendon, K. Motobayashi, S. Ye, M. Osawa, Y. Surendranath, Tracking a common surface-bound intermediate during CO₂-to-fuels catalysis. *ACS Cent. Sci.* **2**, 522–528 (2016).
28. C. M. Gunathunge, X. Li, J. Li, R. P. Hicks, V. J. Ovalle, M. M. Waegle, Spectroscopic observation of reversible surface reconstruction of copper electrodes under CO₂ reduction. *J. Phys. Chem. C* **121**, 12337–12344 (2017).
29. A. S. Malkani, M. Dunwell, B. Xu, Operando spectroscopic investigations of copper and oxide-derived copper catalysts for electrochemical CO reduction. *ACS Catal.* **9**, 474–478 (2019).
30. Y. Zhao, X. Chang, A. S. Malkani, X. Yang, L. Thompson, F. Jiao, B. Xu, Speciation of Cu surfaces during the electrochemical CO reduction reaction. *J. Am. Chem. Soc.* **142**, 9735–9743 (2020).
31. P. Hollins, K. J. Davies, J. Pritchard, Infrared spectra of CO chemisorbed on a surface vicinal to Cu(110): The influence of defect sites. *Surf. Sci.* **138**, 75–83 (1984).
32. P. Hollins, The influence of surface defects on the infrared spectra of adsorbed species. *Surf. Sci. Rep.* **16**, 53–94 (1992).
33. E. Borguet, H.-L. Dai, Site-specific properties and dynamical dipole coupling of CO molecules adsorbed on a vicinal Cu(100) surface. *J. Chem. Phys.* **101**, 9080–9095 (1994).
34. J. Li, K. Chang, H. Zhang, M. He, W. A. Goddard III, J. G. Chen, M.-J. Cheng, Q. Lu, Effectively increased efficiency for electroreduction of carbon monoxide using supported polycrystalline copper powder electrocatalysts. *ACS Catal.* **9**, 4709–4718 (2019).
35. M. Jouny, W. Luc, F. Jiao, High-rate electroreduction of carbon monoxide to multi-carbon products. *Nat. Catal.* **1**, 748–755 (2018).
36. J. Salimon, R. M. Hernández-Romero, M. Kalaji, The dynamics of the conversion of linear to bridge bonded CO on Cu. *J. Electroanal. Chem.* **538–539**, 99–108 (2002).
37. P. Hollins, J. Pritchard, Infrared studies of chemisorbed layers on single crystals. *Prog. Surf. Sci.* **19**, 275–349 (1985).
38. M. Dunwell, J. Wang, Y. Yan, B. Xu, Surface enhanced spectroscopic investigations of adsorption of cations on electrochemical interfaces. *Phys. Chem. Chem. Phys.* **19**, 971–975 (2017).
39. X. Jiang, M. J. Weaver, The role of interfacial potential in adsorbate bonding: Electrode potential-dependent infrared spectra for saturated CO adlayers on Pt(110) and related electrochemical surfaces in varying solvent environments. *Surf. Sci.* **275**, 237–252 (1992).
40. S. L. Yau, X. Gao, S. C. Chang, B. C. Schardt, M. J. Weaver, Atomic-resolution scanning tunneling microscopy and infrared spectroscopy as combined in situ probes of electrochemical adlayer structure: Carbon monoxide on rhodium(111). *J. Am. Chem. Soc.* **113**, 6049–6056 (1991).
41. M. Tüshaus, W. Berndt, H. Conrad, A. M. Bradshaw, B. Persson, Understanding the structure of high coverage CO adlayers. *Appl. Phys.* **51**, 91–98 (1990).
42. L. Wang, S. A. Nitopi, E. Bertheussen, M. Orazov, C. G. Morales-Guio, X. Liu, D. C. Higgins, K. Chan, J. K. Nørskov, C. Hahn, T. F. Jaramillo, Electrochemical carbon monoxide reduction on polycrystalline copper: Effects of potential, pressure, and pH on selectivity toward multicarbon and oxygenated products. *ACS Catal.* **8**, 7445–7454 (2018).
43. A. S. Malkani, J. Li, J. Anibal, Q. Lu, B. Xu, Impact of forced convection on spectroscopic observations of the electrochemical CO reduction reaction. *ACS Catal.* **10**, 941–946 (2020).
44. C. M. Gunathunge, V. J. Ovalle, Y. Li, M. J. Janik, M. M. Waegle, Existence of an electrochemically inert CO population on Cu electrodes in alkaline pH. *ACS Catal.* **8**, 7507–7516 (2018).
45. J. Durst, A. Siebel, C. Simon, F. Hasché, J. Herranz, H. A. Gasteiger, New insights into the electrochemical hydrogen oxidation and evolution reaction mechanism. *Energ. Environ. Sci.* **7**, 2255–2260 (2014).
46. X. Liu, J. Xiao, H. Peng, X. Hong, K. Chan, J. K. Nørskov, Understanding trends in electrochemical carbon dioxide reduction rates. *Nat. Commun.* **8**, 15438 (2017).
47. E. Bertheussen, T. V. Hogg, Y. Abghoui, A. K. Engstfeld, I. Chorkendorff, I. E. L. Stephens, Electroreduction of CO on polycrystalline copper at low overpotentials. *ACS Energy Lett.* **3**, 634–640 (2018).
48. A. Verdaguer-Casadevall, C. W. Li, T. P. Johansson, S. B. Scott, J. T. McKeown, M. Kumar, I. E. L. Stephens, M. W. Kanan, I. Chorkendorff, Probing the active surface sites for CO reduction on oxide-derived copper electrocatalysts. *J. Am. Chem. Soc.* **137**, 9808–9811 (2015).
49. G. Iijima, T. Inomata, H. Yamaguchi, M. Ito, H. Masuda, Role of a hydroxide layer on Cu electrodes in electrochemical CO₂ reduction. *ACS Catal.* **9**, 6305–6319 (2019).
50. R. Subbaraman, D. Tripkovic, D. Strmcnik, K.-C. Chang, M. Uchimura, A. P. Paulikas, V. Stamenkovic, N. M. Markovic, Enhancing hydrogen evolution activity in water splitting by tailoring Li⁺-Ni(OH)₂-Pt Interfaces. *Science* **334**, 1256–1260 (2011).
51. E. Borguet, H.-L. Dai, Strong dynamical dipole coupling between CO molecules adsorbed at two distinct sites on Cu(100). *Chem. Phys. Lett.* **194**, 57–61 (1992).
52. M. M. Sartin, Z. Yu, W. Chen, F. He, Z. Sun, Y.-X. Chen, W. Huang, Effect of particle shape and electrolyte cation on CO adsorption to copper oxide nanoparticle electrocatalysts. *J. Phys. Chem. C* **122**, 26489–26498 (2018).
53. M. Papasizza, A. Cuesta, In situ monitoring using ATR-SEIRAS of the electrocatalytic reduction of CO₂ on Au in an ionic liquid/water mixture. *ACS Catal.* **8**, 6345–6352 (2018).
54. D. K. Lambert, Vibrational stark effect of adsorbates at electrochemical interfaces. *Electrochim. Acta* **41**, 623–630 (1996).
55. I. Persson, Hydrated metal ions in aqueous solution: How regular are their structures? *Pure Appl. Chem.* **82**, 1901–1917 (2010).
56. C. N. Rowley, B. Roux, The solvation structure of Na⁺ and K⁺ in liquid water determined from high level ab initio molecular dynamics simulations. *J. Chem. Theory Comput.* **8**, 3526–3535 (2012).
57. A. Bankura, V. Carnevale, M. L. Klein, Hydration structure of salt solutions from ab initio molecular dynamics. *J. Chem. Phys.* **138**, 014501 (2013).
58. Y. Marcus, Effect of ions on the structure of water: Structure making and breaking. *Chem. Rev.* **109**, 1346–1370 (2009).
59. E. V. Vinogradov, P. R. Smirnov, V. N. Trostin, Structure of hydrated complexes formed by metal ions of Groups I-III of the Periodic Table in aqueous electrolyte solutions under ambient conditions. *Russ. Chem. Bull.* **52**, 1253–1271 (2003).
60. C. M. Choi, J. Heo, N. J. Kim, Binding selectivity of dibenzo-18-crown-6 for alkali metal cations in aqueous solution: A density functional theory study using a continuum solvation model. *Chem. Cent. J.* **6**, 84 (2012).
61. F. A. Christy, P. S. Shrivastav, Conductometric studies on cation-crown ether complexes: A review. *Crit. Rev. Anal. Chem.* **41**, 236–269 (2011).
62. S. E. Weitzner, S. A. Akhade, J. B. Varley, B. C. Wood, M. Otani, S. E. Baker, E. B. Duoss, Towards engineering of solution microenvironments for the CO₂ reduction reaction:

Unraveling pH and voltage effects from a combined density-functional-continuum theory. *J. Phys. Chem. Lett.* **11**, 4113–4118 (2020).

63. Y.-G. Kim, J. H. Baricuatro, A. Javier, J. M. Gregoire, M. P. Soriaga, The evolution of the polycrystalline copper surface, first to Cu(111) and then to Cu(100), at a fixed CO₂RR potential: A study by *operando* EC-STM. *Langmuir* **30**, 15053–15056 (2014).

Acknowledgments

Funding: J.L. and Q.L. acknowledge the National Natural Science Foundation of China (grant no. 21872079). A.S.M. and B.X. acknowledge the support from the National Science Foundation CAREER Program (award no. CBET-1651625). **Author contributions:** A.S.M. performed spectroscopic experiments. A.S.M., N.J.O., X.C., Q.L., and B.X. discussed and analyzed spectroscopic results. J.L. performed reactivity tests. J.L., M.H., B.X., and Q.L. discussed and analyzed reactivity results. B.X. supervised the spectroscopic experiments. Q.L. supervised

the reactivity tests. A.S.M., B.X., and Q.L. wrote the manuscript. All authors edited the manuscript. **Competing interests:** The authors declare that they have no competing interests. **Data availability:** All data needed to evaluate the conclusions in the paper are present in the paper and/or the Supplementary Materials. Additional data related to this paper may be requested from the authors.

Submitted 10 June 2020

Accepted 22 September 2020

Published 6 November 2020

10.1126/sciadv.abd2569

Citation: A. S. Malkani, J. Li, N. J. Oliveira, M. He, X. Chang, B. Xu, Q. Lu, Understanding the electric and nonelectric field components of the cation effect on the electrochemical CO reduction reaction. *Sci. Adv.* **6**, eabd2569 (2020).